Supplementary material

Figure S1. A canonical view of MD recognition. QacR is a MD-binding gene regulator in *S. aureus*. Like many other structurally characterized MDR proteins, QacR employs a large cavity (>1100Å^3) composed of overlapping, distinct "minipockets" in the recognition of structurally unrelated drugs(7). QacR (front and top views) is shown below as gray ribbons. The MD-binding pocket surface was generated using CASTp(38). The QacR pocket is shown bound to crystal violet (yellow sticks), rhodamine (green sticks) and dequalinium (pink sticks), all of which interact with different areas of the large drug-binding cavity. This is in stark contrast to BmrR, which uses a common interaction surface to bind diverse drugs (see Figure 2).

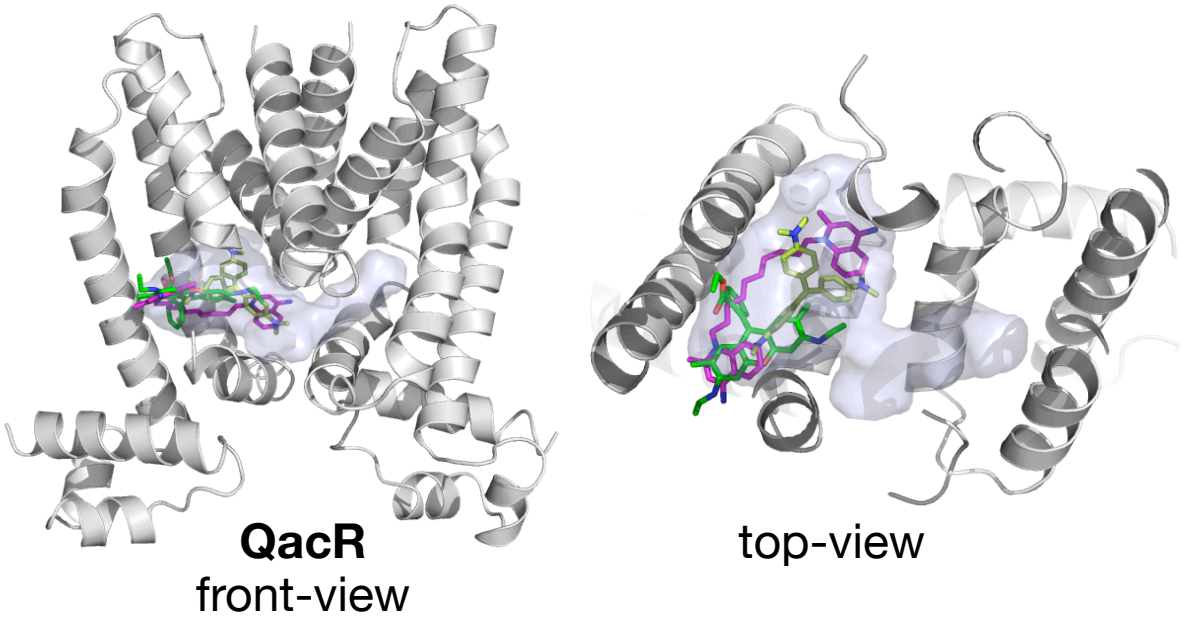

Table S1. Analysis of ligand-docking modes in the refined BmrR models. Ligands were not included in the working models until later stages of the structure refinements. The experimental $2F_o$-F_c and F_o-F_c electron density maps and R-factors were used to guide the modeling of the BmrR probes. The ligand orientations and conformations observed in the final models offered the best real space correlation coefficient. Alternative binding modes did not offer fits to the electron density or improved chemistry. The coefficients were calculated using Phenix crystallography package(17).

LIGAND	real space correlation coefficient
4AQ	0.826
PUR	0.868
ET	0.708
TET	0.753
KAN	0.772
ACH	0.917

Figure S2. Analysis of alternative ACH and ET docking modes. (**A** and **E**) Ligand-docking observed in the refined models of BmrR bound to ACH and ET, respectively. The others include alternative binding modes considered during the refinements.

(**A**-**D**)The refinement of the structure of BmrR bound to ACH afforded electron density much larger than the ACH ligand. To determine the best possible fit, four ACH orientations were modeled into the refined density. The refinement statistics, model quality and real space correlation coefficient were used to select the final assigned binding mode. Refinement was performed using CCP4(16). The real space correlation coefficients were calculated using Phenix(17). Solvent was added after the final ACH orientation was assigned. The solvent-ACH interactions are discussed in Figure S6.

(**E**-**H**) ET binding was modeled with four different docking modes based on the observed excess electron density in the BmrR drug-pocket. After refinement of the BmrR-ET complex, the final ET orientation was selected based on R-free values, real-space correlation coefficients to $2F_o$-F_c maps, and stereochemical/energetic considerations. For example, **F** and **G** were eliminated as feasible candidates based on intramolecular strain, namely between the phenyl and phenantridinium rings. Docking mode **F** also revealed clashes with the side chains of N149, Y187 and E253. Docking **E** was chosen over **H** based on the resulting real-space correlation coefficient and R_{FREE} (24.7% and 25.9%) values.

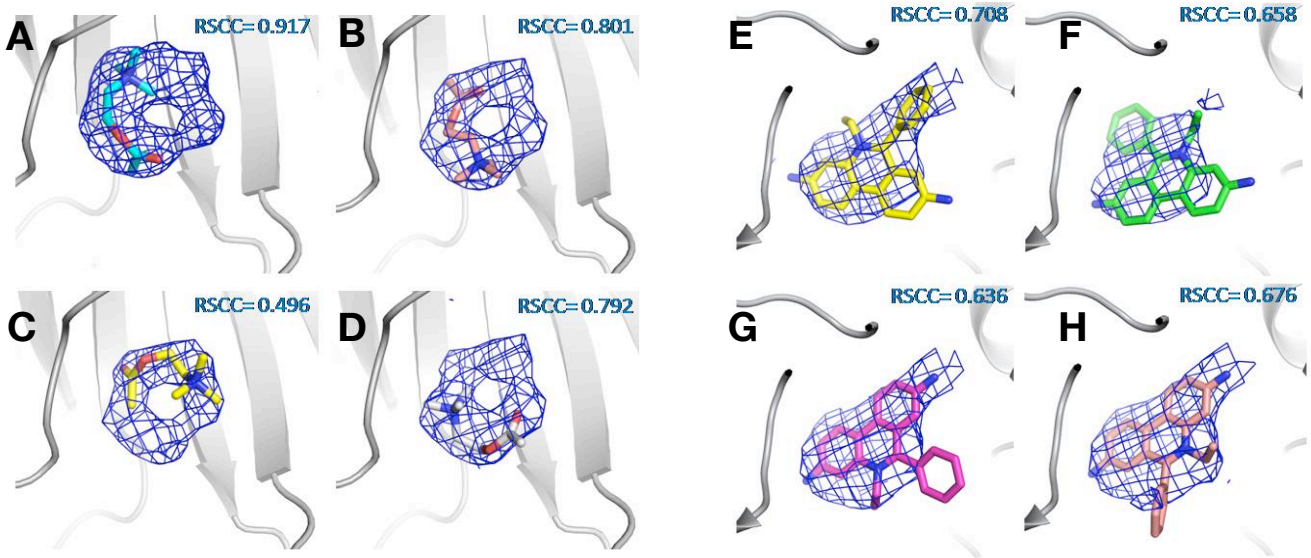

Table S2. A comparison of, binding, ligand burial and shape complementarity in BmrR-drug and specific protein-ligand complexes. All ASA burial data were used to calculate the percent ligand burial values (see Figure 3 legend for description of calculations). The shape complementarity values were calculated using the Sc program of the CCP4 crystallography suite(16).

LIGAND	K_D (M)	% LIGAND ASA buried	Sc
4AQ	2.1 (± 0.56) E-04	76	0.58
ET	1.9 (± 0.2) E-06	75	0.46
TET	5.1 (± 0.5) E-05	81	0.56
PUR	1.7 (± 0.4) E-05	76	0.56
KAN	2.8 (± 0.9) E-05	83	0.57
ACH	6.6 (± 3) E-06	83	0.58
TPP	8.1 (± 0.6) E-05	59	0.60
BER	1 (± 0.2) E-05	75	0.62
RHO6G	5.2 (± 1.0) E-07	74	0.66
TetR:tetracycline pdb code: 2VKE	3.30E-10	86	0.70
avidin:biotin pdb code: 2AVI	1.00E-15	96	0.80
LacI:IPTG pdb code: 2P9H	8.30E-07	98	0.82
RBP:retinol pdb code: 2AVI	7.00E-08	94	0.72

Table S3. A summary of BmrR-ligand interactions. Ligand interactions were analyzed using the ligand-protein contact server (http://bip.weizmann.ac.il/oca-bin/lpccsu)(41). Legend: ● Long hydrophobic contacts (carbon atom separations of 3.5 - 4.5 Å); ●● Close hydrophobic contact (carbon atom separations of 3.0 - 3.5 Å); ■ Aromatic-aromatic interactions; ◆ Ligand to side-chain H-bonding contacts; ▼ Long-range electrostatic interactions between the ligand cationic centers and Glu253

residue	PUR	ET	TET	4AQ	KAN	ACH
Pro144	●	●	●●	●	-	-
Val147	●●	●●	●●	●●	●●	●
Asn149	-	●	◆	-	◆	◆
Tyr152	■◆	●●	●	■	●	●
Tyr170	■◆	●	-	●	●	●
Tyr187	●◆	-	●	■	-	-
Phe224	■	■■	■	■	●	-
Tyr229	■	-	■	■	●	-
Glu253	▼	▼	▼	▼◆	▼◆	▼
Ile255	●●	●●	●●	●●	●●	●●
Tyr268	-	●	●	■	-	●

Figure S3. Schematic representation of BmrR-ligand contacts. Cutoff distances of 4.5 Å and 3.5 Å were used for hydrophobic interactions and H-bonds, respectively. Residues are colored by type: orange (hydrophobic residues), brown (aromatic residues), red (acidic residues), blue (H-bonding, polar residues). H-bonding distances are depicted in green. The figure was generated using the program Ligplot(42).

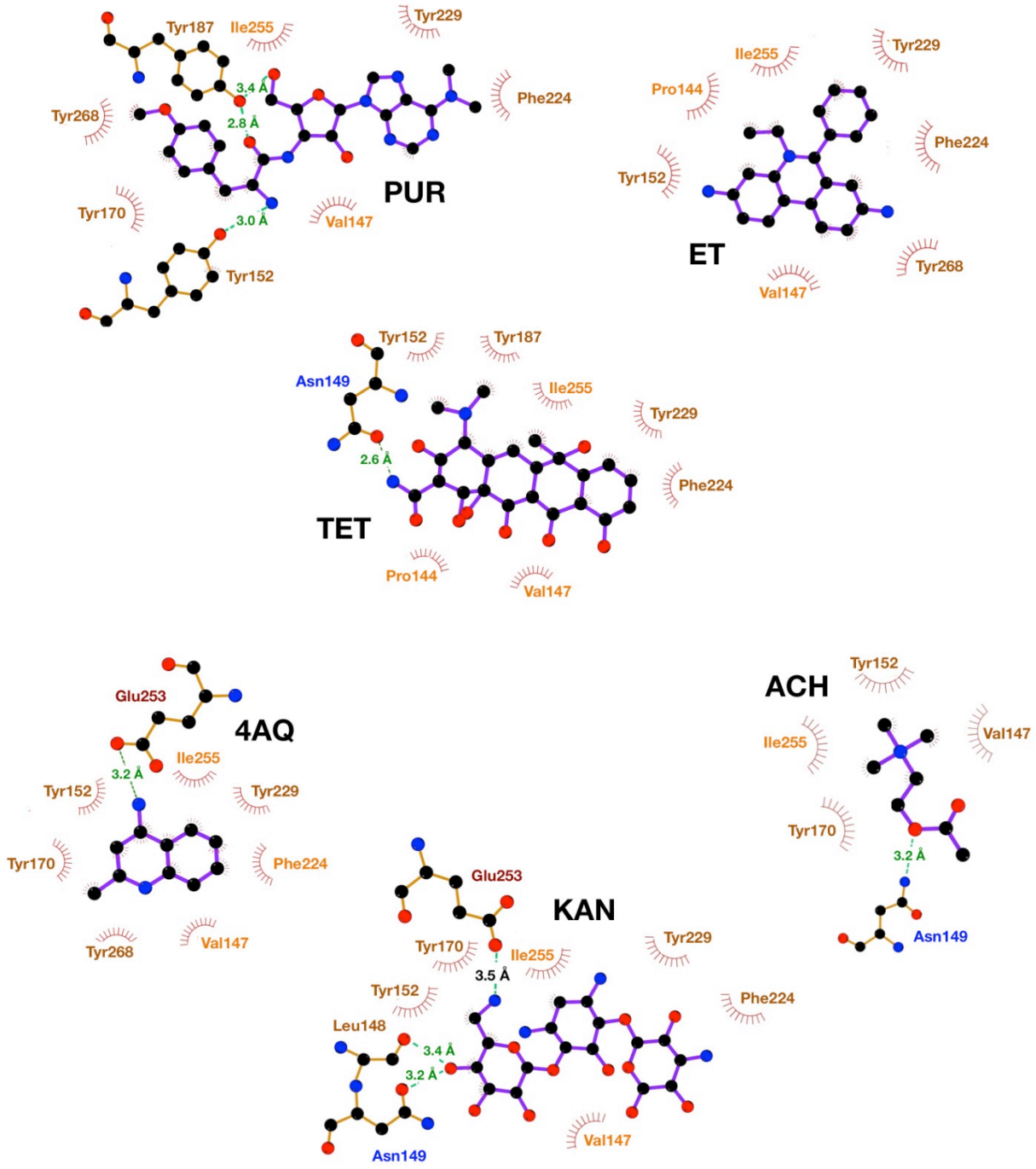

Table S4. Protein and ligand accessible surface area (ASA) burial upon binding to BmrR. The programs NACCESS and AREAIMOL of the CCP4 package were used for the ASA calculations(16). Only the oxygen and nitrogen were considered as polar in the calculation of polar ASA burial.

LIGAND	TOTAL ASA (Å^2)	LIGAND	PROTEIN	LIGAND nonpolar polar	PROTEIN nonpolar polar
4AQ	475	293	181	237 56	138 43
ET	692	408	283	299 164	215 68
TET	755	462	292	324 84	236 56
PUR	829	472	356	351 131	269 89
KAN	812	482	329	188 294	268 62
ACH	499	270	230	250 20	168 62
TPP	668	366	302	366 0	177 125
BER	735	444	291	410 34	218 73
RHO6G	971	597	374	571 26	215 99

Figure S4. Fluorescence quenching studies of MD recognition. All binding curves (right) were generated using corrected fluorescence intensities (λ_{EM} = 305 nm). The ligand K_D values were determined from numerical fits (Kaleidagraph, Synergy Software) to the data. In all cases, the data were best described by the identical, independent single site model (equation 1):

$$F_{obs} = F_{initial} - \Delta F_{max}\left(\frac{[L]}{[L]+K_D}\right) \quad (1)$$

where F_{obs} is the observed fluorescence, $F_{initial}$ is the initial sample fluorescence, ΔF_{max} is the total intensity change over the course of the titraton, [L] is the total ligand concentration and K_D is the dissociation constant. For all titrations [BmrR] << K_D. The $F_{initial}$ and ΔF_{max} values were determined for each experiments. The affinity constants shown in Table 1 are averaged values from at least two independent determinations. Standard analyses was used in the propagation of errors(43).

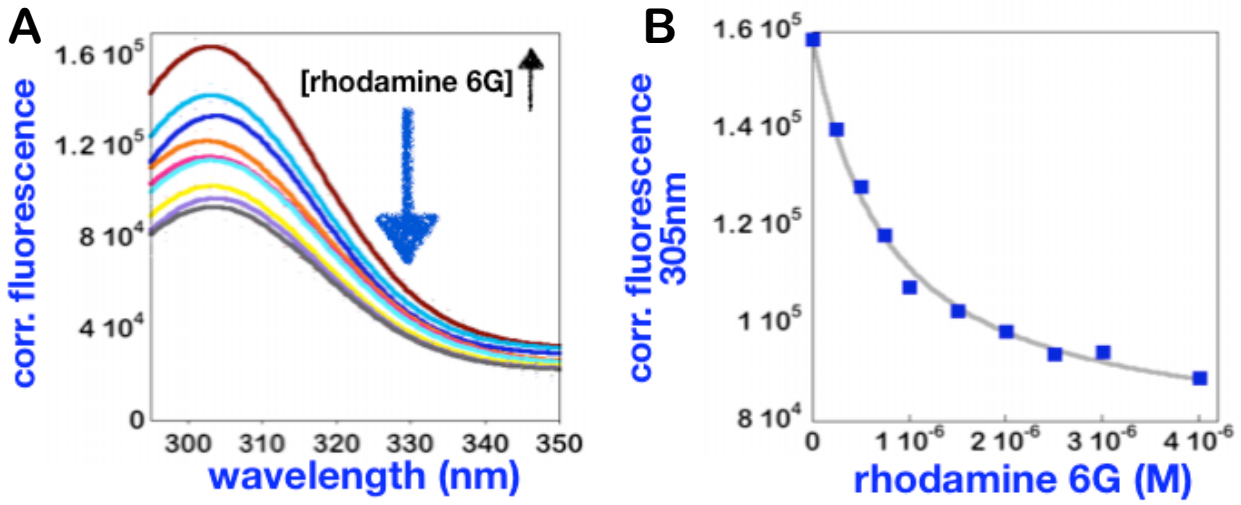

Fluorescence quenching studies: experimental. Fluorescence data were collected on a ISS (Chronos) fluorimeter using the intrinsic BmrR fluorescence (λ_{EX} = 285 nm) at 25°C in 25mM potassium phosphate, 200mM KCl, 1mM EDTA, 2mM DTT and 5% glycerol (spectrophotometric grade), pH 7.5. BmrR dimer concentrations (determined by UV-Vis), for the K_D determinations, ranged from 100 to 300 nM. The protein ε_{280} value was calculated using ProtParam. All BmrR (1-10 mM) and ligand (250µM-10mM) stocks were prepared in the fluorescence buffer. Gel filtration PD-10 columns, (GE Healthcare) was used to change buffer systems. All titration experiments included fluorescence and UV-Vis measurements of working and reference samples. Ligands were added to the working and reference samples in stepwise fashion (1-20 µM aliquots of 0.25-10 mM stocks). Fluorescence and UV-Vis spectra were collected after a 2-5 minute equilibration time. Corrected intensities were obtained after dilution, inner filter effects and background corrections were applied. Inner filter corrections were applied when the solution absorbance at the excitation wavelength was greater than 0.1. The starting sample volumes were 2.5 mL. The final values did not exceed 2.8mL.

Figure S5. Chemical structures of BmrR probes employed in previously reported X-ray and solution-binding studies(6,13, 23)**.**

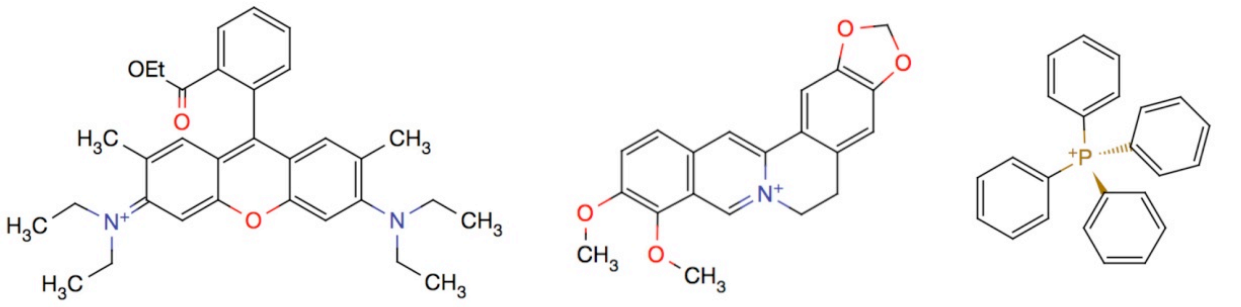

rhodamine 6G (RHO6G) berberine (BER) tetraphenylphosphonium (TPP)

Figure S6. Correlations of drug binding with ligand burial. Plot of $\ln K_D$ vs sum of the total ligand ASA buried (**A**) and non-polar ligand ASA (**B**) buried by ligands binding to BmrR display linear correlations with slopes of -6.03 ± 3.0 (R = 0.550) and -6.23 ± 2.3 (R = 0.644) cal/(mol•Å^2), respectively. Surface area was calculated using the program NACCESS and AREAIMOL of the CCP4 package(17). (**C**) Plot of $\ln K_D$ vs sum of the total ligand ASA buried for the QacR system displays a linear correlation of -7.9 ± 2.2 (R = 0.637) cal/(mol•Å^2).

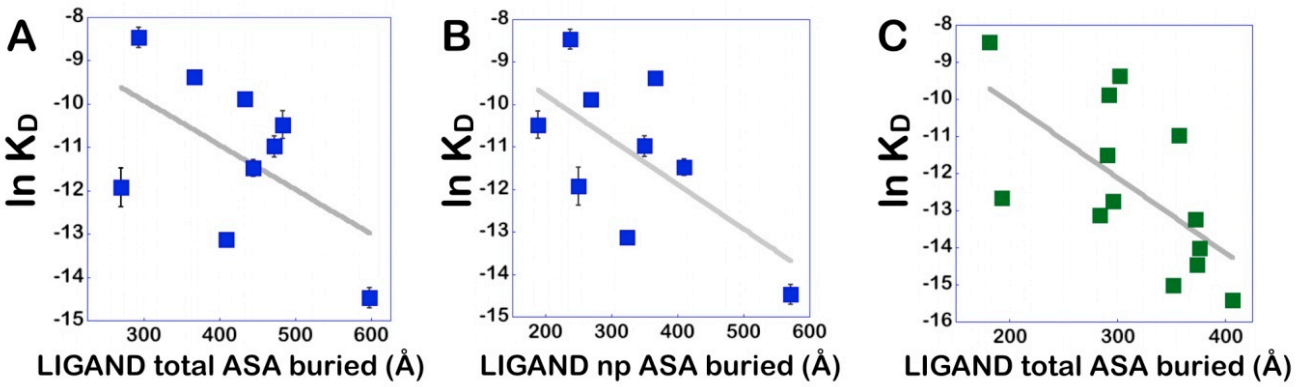

Figure S7. Ligand efficiencies in BmrR. The plot below presents the relationship between compound potency and the size of the BmrR ligands. The binding free energy (-ΔG) is plotted against the number of non-hydrogen atoms (see ref. 31). The ligand K_D values were converted to free energies using a standard state of 1M at 298K. The slope obtained from the linear fit ΔG = slope x (number of non-hydrogen atoms) is 0.22 and the correlation coefficient is 0.54. The near linear relationship implies a uniform ligand efficiency for these targets. Note ACH shows the largest deviation from the relationship and binds more tightly than predicted. The origins for observed ACH affinity is unknown at this time.

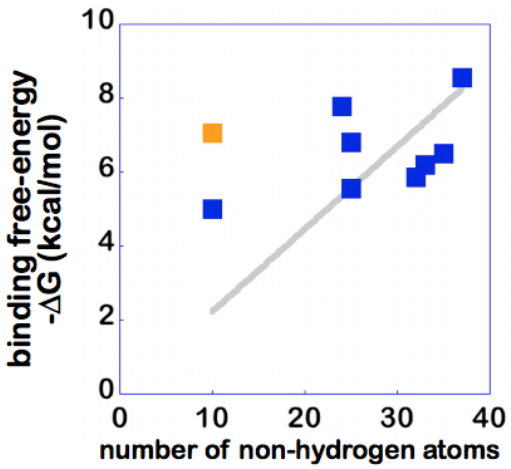

Figure S8. Qualitative analyses of binding and polar ASA burial. (A) Total (ligand + protein) polar ASA burial (B) Protein polar ASA buried (C) Ligand polar ASA buried. All polar ASA values were calculated in NACCESS. Only the oxygen and nitrogen atoms were considered as polar atoms in calculations. See Figure S5 legend for calculation details.

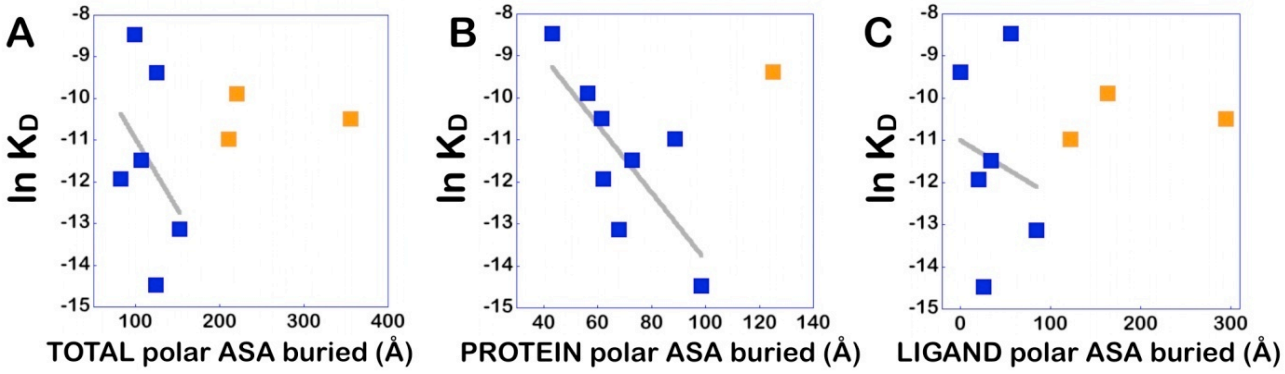

Figure S9. Acetylcholine-water interactions. The 1.95 Å structure of L-ficolin (PDB code: 2J0H, Garlatti V*, et al.* (2007) *EMBO J* 26:623-633) bound to acetylcholine and N-acetylglucosamine ligands presents two examples (**B** and **C**) of acetylcholine-solvent interactions that are relevant to those observed in the X-ray structure of BmrR bound to ACH (**A**). The BmrR and L-ficolin backbone and side-chains are depicted in gray as ribbons or sticks. All acetylcholine molecules are depicted as green sticks. The solvent molecules are depicted as red spheres. All nitrogen and oxygen atoms are colored blue and red, respectively. All examples show the quaternary amine group interacting with water molecules with similar (O••N) distances.

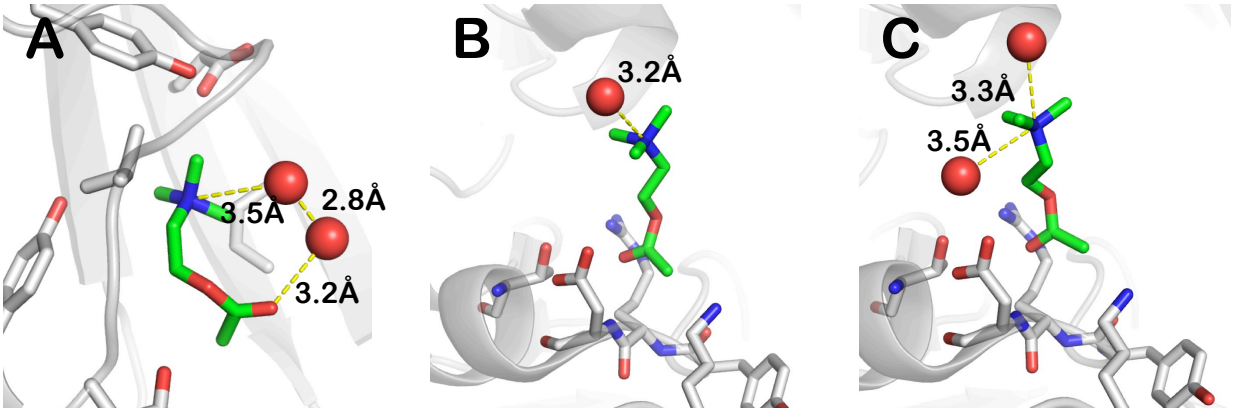

Figure S10. H-bonding capacity for the BmrR drug-pocket. H-bonding oxygen and nitrogen atoms identified in the BmrR X-ray structures solved to date are shown as small red and blue spheres, respectively. H-bonding interactions have not been observed for the atoms highlighted as violet spheres, though these atoms are located within 4 Å of bound ligands and are thus potential candidates for donating and accepting H-bonds.